

THE TOPOLOGY OF REIONIZATION

KHEE-GAN LEE, RENYUE CEN, J. RICHARD GOTT III AND HY TRAC
Department of Astrophysical Sciences, Princeton University, Princeton, New Jersey 08544, USA
To be submitted to ApJ

ABSTRACT

Using the largest cosmological reionization simulation to-date (~ 24 billion particles), we use the genus curve to quantify the topology of the neutral hydrogen distribution on scales $\geq 1 \text{ Mpc } h^{-1}$ as it evolves during cosmological reionization. We find that the reionization process proceeds primarily in an inside-out fashion, where higher density regions become ionized earlier than lower density regions. There are four distinct topological phases: (1) Pre-reionization at $z \gtrsim 15$, when the genus curve is consistent with a Gaussian density distribution. (2) Pre-overlap at $10 \lesssim z \lesssim 15$, during which the number of HII bubbles increases gradually with time, until percolation of HII bubbles starts to take effect, characterized by a very flat genus curve at high volume fractions. (3) Overlap at $8 \lesssim z \lesssim 10$, when large HII bubbles rapidly merge, manifested by a precipitous drop in the amplitude of the genus curve. (4) Post-overlap at $6 \lesssim z \lesssim 8$, when HII bubbles have mostly overlapped and the genus curve is consistent with a diminishing number of isolated neutral islands. After the end of reionization ($z \lesssim 6$), the genus of neutral hydrogen is consistent with Gaussian random phase, in agreement with observations.

Subject headings: cosmology: theory — intergalactic medium — large-scale structure of universe — methods: numerical — methods: statistical — radiative transfer

1. INTRODUCTION

Two recent major observational milestones combine to suggest that the so-called “dark ages” of the universe (Peacock 1992; Rees 1998) may be rather complex. The first major milestone was laid down by the recent absorption spectrum observations of high redshift quasars from the Sloan Digital Sky Survey (SDSS), indicating that the final reionization episode came to completion at $z \sim 6$ (see 3; 6; Barkana 2002; Cen & McDonald 2002; 15).

The Wilkinson Microwave Anisotropy Probe (WMAP) polarization observations, probing the ionization state of intergalactic medium (IGM) in the high redshift universe, set the second major milestone. The WMAP observations indicate $\tau_e = 0.09 \pm 0.03$ (23), suggesting that the process of reionization occurred at redshifts considerably greater than $z \sim 6$, possibly $z \geq 15$, although the current uncertainty in τ_e allows a very wide range of reionization histories.

Although the complex reionization process implied by these observations did not appear as a total surprise (e.g., Gnedin 2000b; Barkana & Loeb 2001; Madau 2002; Wyithe & Loeb 2003; 16; Cen 2003; 25; 22; 5; Venkatesan & Truran 2003; Ricotti & Ostriker 2004), it is unclear at this time how the universe had actually evolved from $z \sim 1000$ to $z = 6$, for different scenarios could be designed to arrive at the same observed total Thomson optical depth (e.g., 14) as well as satisfy the sudden rise in ionizing radiation background observed at $z \sim 6$.

Thus, at present, many details of the cosmological reionization process are still unknown. It is expected, however, that upcoming observations at various observational bands from radio to optical promise to provide

much more refined statistical information than what is available today. Therefore, advances on the theoretical side are demanded in order to provide both useful insights and a quantitative framework for the interpretation of future observations.

At present, we make the first attempt to quantify the topological evolution of cosmological reionization, in the context of the conventional scenario that stellar radiation is primarily responsible for reionizing the universe. We utilize a state-of-the-art cosmological reionization simulation of a box size $100 \text{ Mpc } h^{-1}$, which involves a hybrid algorithm inclusive of detailed radiative transfer (Trac & Cen 2006; 21). This paper is organized as follows: the method section describes the genus and simulation code, followed by a description of the results and the manner in which they are presented. We then give a detailed discussion of the changes in the topology of the neutral fraction at different stages of reionization.

2. METHOD

2.1. Genus: A quantitative measure of topology

In order to study the topology of a three-dimensional data set like those in the simulation, we must first specify two-dimensional contours. From a continuous density distribution, this can be done by defining contours of constant density at different volume fractions f , i.e. the fraction of the volume occupying the high-density side of the contour. The topology of contours at a given threshold density can then be quantified with the genus.

For a Gaussian distribution,

$$f = \frac{1}{\sqrt{2\pi}} \int_{\nu}^{\infty} e^{-x^2/2} dx \quad (1)$$

(13), where $\nu = \delta/\xi(0)^{1/2}$ is the number of standard deviations by which the threshold density δ of the contour departs from the mean density in a Gaussian distribution

with covariance function $\xi(r)$. For example, the density contour with $\nu = 1.5$ is that which encloses $\sim 93\%$ of the volume, or $f = 0.07$ (i.e. 7% of the volume has a higher density than $\nu = 1.5$).

While the relation between f and ν as defined in Equation 1 holds only for a Gaussian distribution, it has become the convention to use ν as a convenient label for the different density contours when studying the genus of a distribution, even if the distribution is not Gaussian. In order to allow comparisons with the published literature dealing with the genus, we will mostly follow this convention of referring to contours using ν as a label, which is related to the actual volume fraction f by Equation 1. This also has the advantage that large values of ν intuitively correspond to high threshold densities and vice-versa, whereas f decreases with increasing threshold density.

Mathematically, the topology of an object is defined by its homeomorphism, i.e. its geometric properties under deformations and not transformations which ‘break’ an object or ‘connect’ it with others (see, e.g. Seifert & Threlfall 1980). One quantitative measure of an objects topology is its genus (13; 8; 11). We define the genus of a repeating or infinite contour as

$$G_s = (\text{no. of holes}) - (\text{no. of isolated regions}) \quad (2)$$

where a ‘hole’ is like that in a torus, while an ‘isolated region’ can be either above or below the threshold density of a contour (8). In this paper we define ‘holes’ and ‘isolated regions’ depending on whether the threshold density of the contour being studied is higher or lower than the 50% median density value: for voids, isolated regions are defined as those with lower densities than the threshold density, while the reverse is true for dense pockets.

Thus, a single dense region in an empty box and a single void in a solid box are both counted as ‘isolated regions’ and are hence topologically equivalent. This allows for a symmetry in the definition of the genus for low density ($\nu < 0$) and high density ($\nu > 0$) regions.

The genus of a repeating or infinite two-dimensional contour can be calculated by integrating its Gaussian curvature K over the entire area A ,

$$G_s = \frac{-1}{4\pi} \int K dA \quad (3)$$

where the Gaussian curvature is defined as the reciprocal of the two principle radii of curvature a_1 and a_2 at the point, i.e. $K \equiv 1/(a_1 a_2)$ (13; 8). As an illustration, take for example a density contour which comprises of 20 isolated spheres, each of radius r_s . The Gaussian curvature at any point on the surface of each sphere is $K = r_s^{-2}$, while the total surface area is of course $20(4\pi r_s^2)$. Using Equation 3 gives a genus of -20 as we would expect from the definition given in Equation 2. A multiply-connected, sponge-like contour would have a positive genus value, since the two principal radii of curvature on its surface tend to point in opposite directions rather than in the same direction, giving it a negative curvature. In a three-dimensional data set where each data pixel is essentially a cube, the genus is calculated by summing up the angle deficits at the vertices of the Lego-like contour surface. We use a computer program, CONTOUR3D, written by

(**author?**) (Weinberg 1988) for this purpose.

A point worth noting is that since the genus is calculated over the entire volume of the box, a combination of multiply-connected structures and isolated pockets could lower the amplitude of the genus. We thus have to be careful in distinguishing between, say, a volume with one figure-8 shaped object plus three small isolated spheres in it, as opposed to another volume with just one large isolated sphere, since both situations will give a total genus of -1.

The genus provides a useful tool for probing the relative connectedness of high- and low-density regions in the large-scale structure of the universe, for scalar quantities such as the dark matter distribution or density of HI. In addition to being dependent on the underlying distribution, the topology of large-scale structure also depends on the density threshold specified for a given contour surface. In general, contours of low threshold densities (i.e. voids occupying lowhigh volume fractions) have a different topology from contours of high threshold density (i.e. dense regions occupying low volume fractions) within a given data set. This provides an additional degree of freedom with which to study the topology of a density distribution, since we can now study the systematic variation of $G_s(\nu)$ with threshold densities using ‘genus curves’.

In addition, the genus is an useful cosmological statistic for another reason. The standard big bang-inflationary model predicts that small-amplitude density fluctuations arise from a random phase Gaussian distribution (2; 1). For such a distribution, the mean genus per unit volume $g_s \sim G_s/V$ is given by a simple analytic expression (Doroshkevich 1970; Adler 1981; 13):

$$g_s = N(1 - \nu^2) e^{-\nu^2/2} \quad (4)$$

where the normalization N as function of wavenumber k is given by

$$N = \frac{1}{4\pi^2} \left(\frac{\langle k^2 \rangle}{3} \right)^{3/2} = \frac{1}{4\pi^2} \left(\frac{\int k^2 P'(k) d^3k}{3 \int P'(k) d^3k} \right)^{3/2} \quad (5)$$

where $P'(k) = P(k) e^{-r^2/2r_{sm}^2}$ is the power spectrum which has been smoothed with a smoothing radius r_{sm} . We thus see that any Gaussian random-phase density distribution would have a curve of $g_s(\nu)$ with the same distinctive shape regardless of the power spectrum, which enters only through the amplitude. The implication is that the shape of the genus curve would remain unchanged through linear evolution of the fluctuations. The initial conditions of our simulation at $z \sim 25$ display this characteristic curve (top left panel, Figure 2), and it is virtually indistinguishable from the theoretical curve.

Equation 4 also shows that there is a symmetry between positive and negative ν in a random phase distribution, i.e. high- and low-density regions with the same absolute value of ν would have an identical topology. For $|\nu| > 1$ (i.e. $f < 16\%$ or $f > 84\%$), the high- and low-density regions would comprise of isolated dense pockets and voids respectively as indicated by the negative genus. The median density contour with $\nu = 0$ or $f = 0.5$, on the other hand, has a positive genus indicating a sponge-like, multiply connected structure (8; 11).

Historically, the genus has provided strong evidence in

support of the Gaussian random phase hypothesis (and hence the now-standard inflationary big-bang model). Studies on the topology of large-scale structure as observed in galaxy surveys have yielded genus curves in remarkable agreement with the form shown in Equation 4, apart from small-scale deviations due to non-linear gravitational effects and biasing from galaxy formation (10; 19; 26; 4; 9). In the present context, this means that the genus is a powerful and sensitive probe of the topology of the neutral fraction in the universe, as reionization causes a departure from a Gaussian random phase distribution.

2.2. Simulations

We use the largest simulation of cosmic reionization run to date (Trac & Cen 2006; 21). It was run with a hybrid code containing a N-body algorithm for dark matter, prescriptions for baryons and star formation, and a radiative transfer (RT) algorithm for ionizing photons. Here we summarize the main simulation parameters.

The hybrid simulation was run with the cosmological parameters: $\Omega_m = 0.26$, $\Omega_l = 0.74$, $\Omega_b = 0.044$, $h = 0.72$, $\sigma_8 = 0.77$, and $n_s = 0.95$, based on the latest results from WMAP, SDSS, BAO, SN, and HST (see ? , and references therein). In a $100 \text{ Mpc } h^{-1}$ simulation box, a high resolution N-body calculation for 2880^3 (i.e. 23.9 billion) dark matter particles on an effective grid with 11520^3 cells is performed using a particle-multi-mesh code (Trac & Pen 2006). With a particle mass resolution of $3.02 \times 10^6 M_\odot h^{-1}$, halos can be reliably resolved down to masses of $\sim 10^8 M_\odot h^{-1}$, accounting for the majority of photoionizing sources.

The radiative transfer of ionizing radiation was run simultaneously with the N-body calculations using a RT grid with 360^3 cells. However, the ionization and recombination calculations were done for each particle individually rather than on the grid to preserve small-scale information down to scales of several comoving kpc h^{-1} . For post-processing, the dark matter, baryons, and radiation are collected on a grid with 720^3 cells and the data is saved every 10 million years from $z = 25$ down to $z = 5$.

3. RESULTS

In the present work, we study the density distribution of neutral hydrogen (HI) at various redshifts during the epoch of reionization. The redshift evolution of the volume- and mass-weighted HI fractions are shown in Figure 1. In our simulation, we can not resolve the damped Lyman alpha systems associated with cooled neutral gas in halos above the cooling mass. Furthermore, we can only account for Lyman limit systems in the form of neutral gas in partially self-shielded mini-halos down to about half a dex in mass below the cooling mass. Thus our HI densities are representative of the IGM and partially exclusive of collapsed regions. We have chosen values for the star formation efficiency and radiation escape fraction such that complete reionization is achieved by $z \sim 6$, as suggested by observations of Lyman alpha absorption in high redshift quasars. The results of our analysis can also be applied to other reionization histories since recent work (28; 17) have shown that the distribution of HI is, in general, similar for different reionization

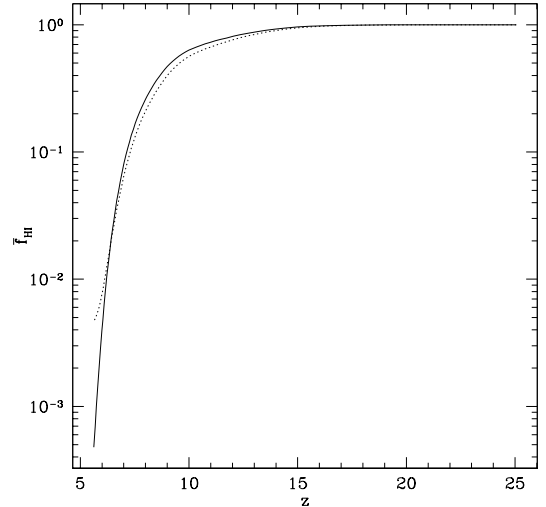


FIG. 1.— The volume-weighted (solid) and mass-weighted (dotted) mean HI fractions from our simulation plotted as a function of redshift. These enable our results to be applied to other reionization histories by matching the mean HI fractions at different epochs.

histories when compared at the same ionization fraction. We thus use the volume-weighted ionization fraction f_{HI} in our plots as an alternative label for different epochs in addition to the redshift z .

The $100 \text{ Mpc } h^{-1}$ simulation box has 720^3 cells, i.e. a spatial resolution of $\sim 0.14 \text{ Mpc } h^{-1}$. Before beginning the analysis, we first smooth the data via a Fourier transform with a Gaussian kernel $W = e^{-r^2/2r_{\text{sm}}^2}$. We use a smoothing length of $r_{\text{sm}} = 1 \text{ Mpc } h^{-1}$, a scale which is adequate to smooth over individual pixels without washing out the structure of HII bubbles during reionization.

We apply the CONTOUR3D code to the simulation results at redshifts ranging from $z \sim 25$, well before the reionization process, to $z \sim 5.5$, after the end of reionization. Figure 2 shows the genus curves of the HI distribution at 9 different redshifts during reionization. These particular redshifts are shown as they represent the ‘turning points’ in the evolution of the topology, and the change between any two adjacent redshifts plotted in Figure 2 is approximately monotonic.

Before we present the detailed discussion, we note that the actual HI threshold density $\rho_{\text{thres, HI}}$ corresponding to a given volume fraction will not, in general, be constant as the universe evolves. As there is a spatial dependence on when neutral regions get reionized, an initially underdense HI region could very well become a dense region relative to the rest of the reionized universe at a later time. We thus need to keep track of the redshift and spatial variation of the threshold density values in order to correctly interpret the changes in topology.

For example, in the initial conditions at $z = 25$ before the onset of reionization, the median HI density at $\nu = 0$ or $f = 0.5$ is essentially the same as the overall mean hydrogen density, i.e. $\rho_{\text{thres, HI}}/\langle\rho_{\text{H}}\rangle \approx 1$ (recall that for a Gaussian distribution, ν is the number of standard deviations from the mean, so the median 50% volume fraction threshold density is the same as the mean density at $\nu = 0$). By the end of reionization at $z \sim 6$, the average neutral fraction is close to zero, so

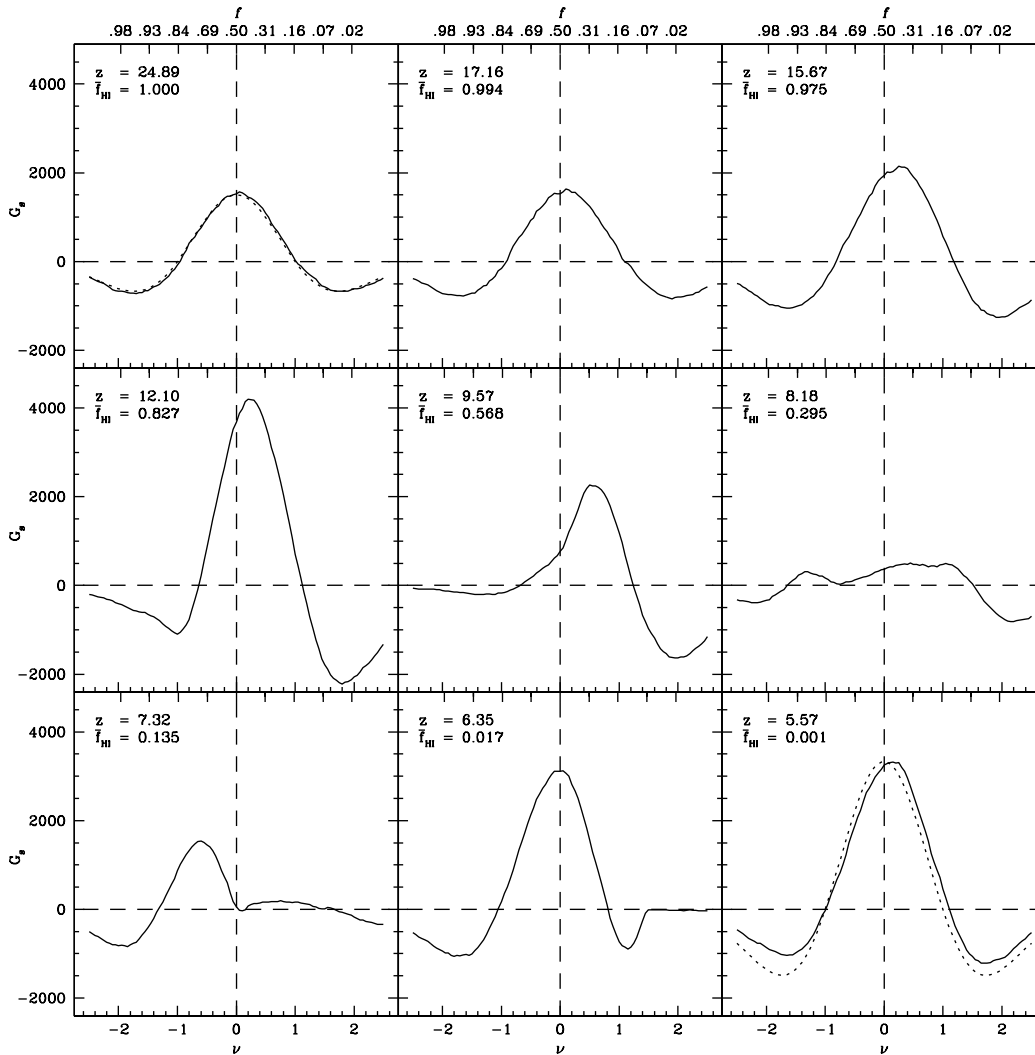


FIG. 2.— Genus curves of the HI density distribution at various epochs during reionization, labeled by redshift z and corresponding volume-weighted mean neutral hydrogen fraction \bar{f}_{HI} . Following convention, we label the bottom axes with the quantity ν which is related to the volume fraction f (on top axes) by Equation 1 (see discussion in text). The dotted curves plotted in the top-left and bottom-right panels are the best-fit theoretical curves for a Gaussian random-phase distribution (Equation 4). The vertical and horizontal dashed lines provide fiducial points for $\nu = 0$ and $G_s = 0$ respectively.

$\rho_{\text{thres, HI}}/\langle\rho_{\text{H}}\rangle \approx 0$. While we expect the densities in general to fall as reionization progresses, from Figure 3 it is obvious that $\rho_{\text{thres, HI}}$ for different values of ν decrease at different rates during reionization, and at different redshifts. We thus need to keep track of the evolution and spatial variation of the actual threshold density values corresponding to a given ν in order to correctly interpret the changes in topology.

Another property we can study with the genus analysis is the characteristic scale of the neutral structures at a given epoch. From Equations 4 and 5, the amplitude N of a Gaussian distribution's genus curve is related to the cube of its root-mean-squared (r.m.s.) wavenumber $\langle k^2 \rangle^{1/2}$. We thus have an estimate of the characteristic scale of a Gaussian distribution by inverting Equation 5 to calculate $\langle k^2 \rangle^{1/2}$ from the amplitude $G_{s, \text{peak}}$ of the genus curve.

Even if the distribution is not exactly Gaussian random-phase, the maximum amplitude of the genus curve can still give information about its characteristic scale at higher densities so long as the distribution remains approximately Gaussian around those higher densities. As an analogy to illustrate this argument, consider a sea sponge immersed in water. When the sponge is moved to dry land, the topology of the enclosed volume, evaluated at the density of water, will change drastically as water drains and evaporates away. At the density of the sponge itself however, there will be little change in the topology compared with when it was immersed in the sea. Similarly, even as ionized bubbles begin growing in the simulation box, we can still use the amplitude of the higher density regions as an indication of scale so long as the bubbles do not occupy a major fraction of the volume.

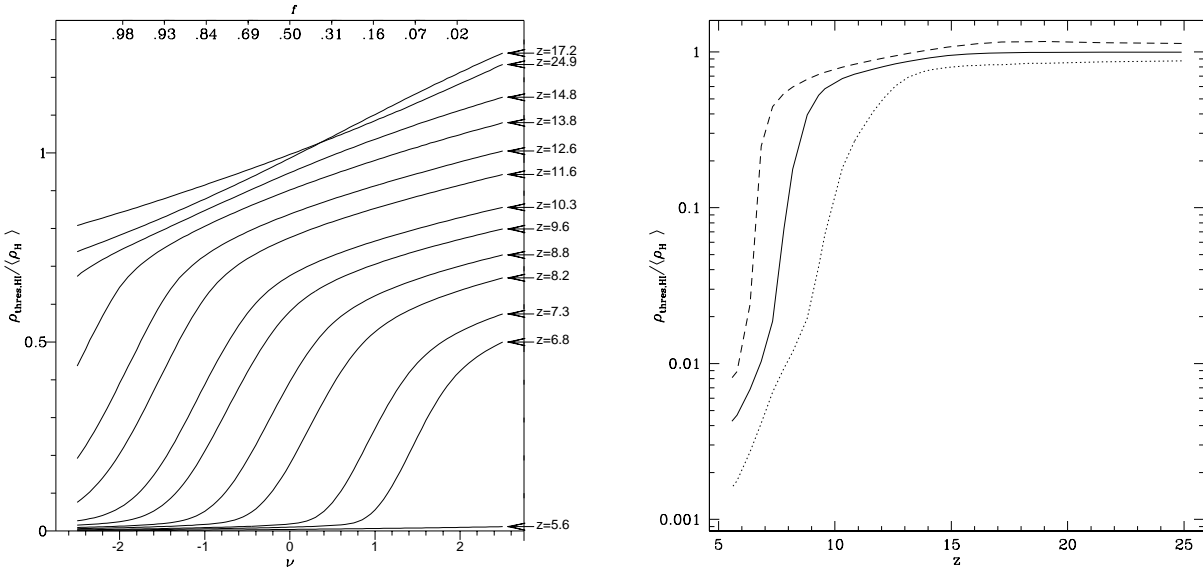


FIG. 3.— (a) Left panel shows the contour threshold densities as a function of ν , (or equivalently volume fraction f ; see Equation 1), at different redshifts. Note that the threshold densities do not decrease monotonically in the early phases, between $z \sim 25$ and $z \sim 17$ (see discussion in text) (b) Right panel shows the redshift evolution of the threshold densities at $f = 0.93$ or $\nu = -1.5$ (dotted line), $f = 0.5$ or $\nu = 0$ (solid line) and $f = 0.07$ or $\nu = 1.5$ (dashed line).

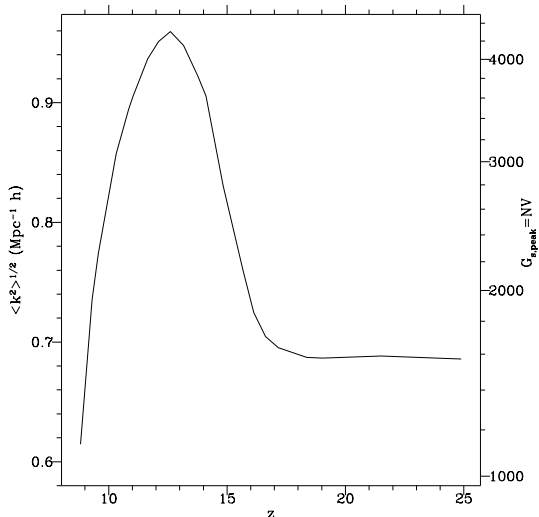


FIG. 4.— The r.m.s wavenumber of the HI distribution, plotted as a function of redshift. The right axis labels f the corresponding genus amplitudes $G_{\text{s,peak}}$ for our simulation volume (see Equation 5). We truncate the plot at around the epoch when the topology departs strongly from a Gaussian distribution, at $z \sim 8$ (see discussion in text).

A cursory glance at Figure 2 shows that even when the topology deviates from the W-shaped Gaussian curve, if we ignore the negative ν (i.e. low-density) part of the genus curves, the high-density part does indeed retain an approximately Gaussian shape down to $z \sim 10$. For example, the $\nu \gtrsim -1$ portion of the $z = 12.1$ curve looks like part of an off-center Gaussian curve. Immediately after $z \sim 10$, the topology of the distribution becomes completely non-Gaussian (e.g. $z = 8.2$ curve in Figure 2) and it becomes difficult to define the amplitude of the peak. We plot the genus amplitude $G_{\text{s,peak}} = NV$ (for a box volume $V = 100^3 \text{ Mpc}^3 h^{-3}$) and the corresponding $\langle k^2 \rangle^{1/2}$ at redshifts $9 \lesssim z \lesssim 25$ in Figure 4.

4. DISCUSSION

In this section, we present a detailed analysis of the different phases of reionization identified from the variation in the topology of the HI density. In particular, we have identified processes corresponding to ‘pre-overlap’, ‘overlap’ and ‘post-overlap’ reionization first described by (author?) (Gnedin 2000a).

4.1. Pre-reionization; $z \gtrsim 16$; $\bar{f}_{\text{HI}} \gtrsim 0.96$

As the pre-ionization universe is completely neutral at $z \sim 25$, the topology of the HI distribution is that of the primordial Gaussian random phase distribution (top-left panel of Figure 2). The HI density contours of this distribution are illustrated in the top-left panel of Figure 5 (for clarity, we only show a $25 \text{ Mpc } h^{-1}$ section extracted from the overall $100 \text{ Mpc } h^{-1}$ box). Both high- and low-density contours are split into similar numbers of isolated regions corresponding to a negative genus, while the median density contour at $\nu = 0$ or $f = 0.5$ is essentially one multiply-connected object with many holes in it, giving a positive genus.

While star-formation is already occurring during this epoch, the star-formation rate $\text{SFR} \lesssim 10^{-3} \text{ M}_{\odot} \text{ Mpc}^{-3} \text{ yr}^{-1}$ is too small to provide significant ionizing flux to the IGM; we see from Figure 1 that $\bar{f}_{\text{HI}} \approx 1$. Hence, the dominant effect on the neutral gas distribution in this era is linear gravitational evolution.

In Figure 3, we see that throughout this epoch the HI threshold density at $\nu = 0$ or $f = 0.5$ remains almost the same as the mean density of all hydrogen in the universe, $\rho_{\text{thres, HI}}/\langle\rho_{\text{H}}\rangle \approx 1$. Indeed, as the universe evolves during this time, the densities of regions with $\nu > 1$ actually increase relative to the early conditions at $z \sim 25$ while the densities of the voids with $\nu < 1$ decrease slightly. Both curves however remain straight lines. This behaviour is as expected from linear evolution: the dense regions cluster due to gravitational interactions at the expense of the underdense voids. This

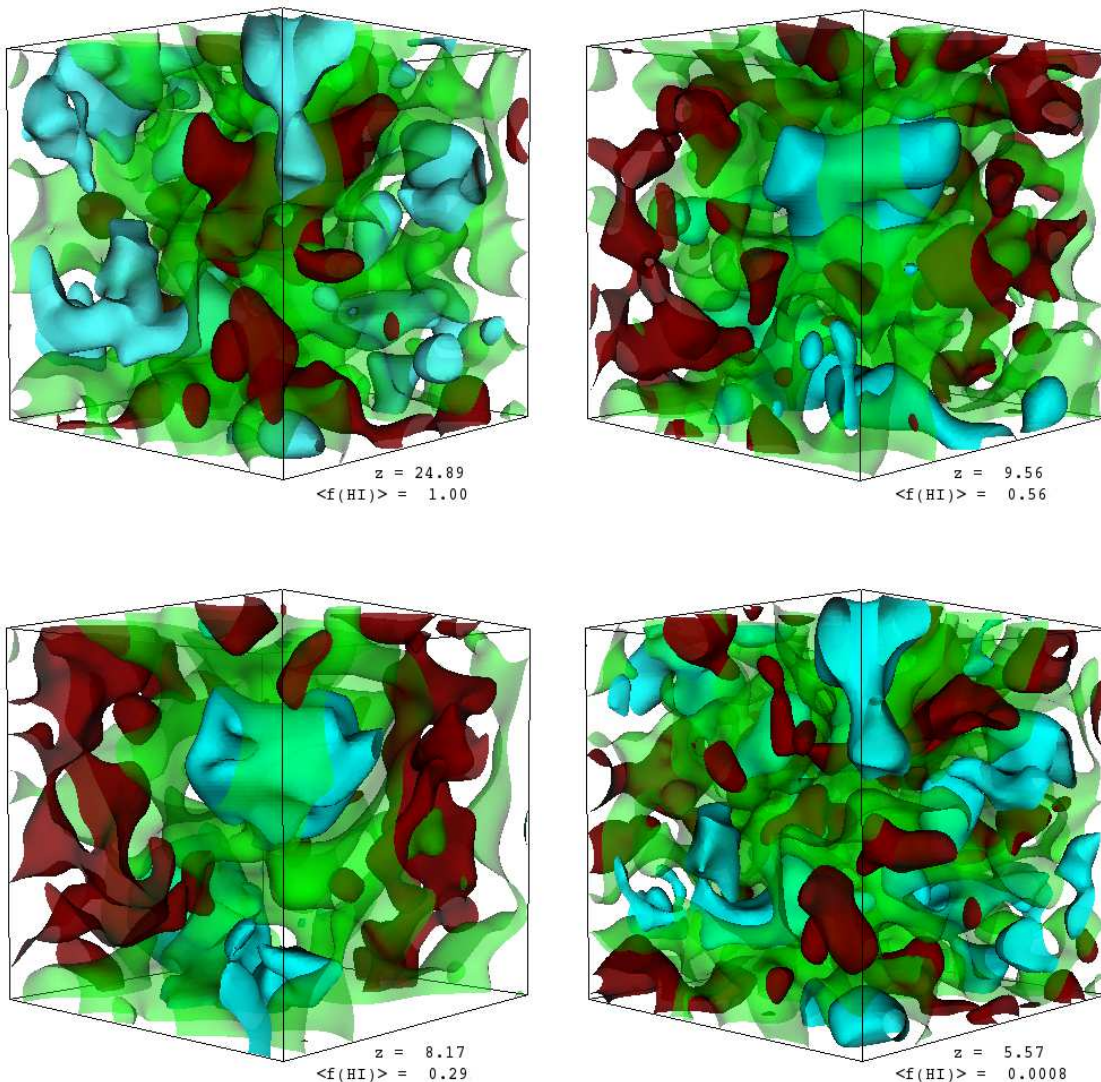


FIG. 5.— HI density contours from a $25 \text{ Mpc } h^{-1}$ subsection of the overall $100 \text{ Mpc } h^{-1}$ simulation box, labeled by redshifts and their corresponding volume-weighted mean neutral fractions. The different colors correspond to densities occupying different volume fractions at that redshift. Blue: $f = 0.93$ or $\nu = -1.5$; green: $f = 0.5$ or $\nu = 0$; red: $f = 0.07$ or $\nu = 1.5$. Note that actual threshold density values vary with redshift (see discussion in text).

leaves the topology essentially unchanged, as can be ascertained by comparing the plot for $z = 17.2$ in Figure 2 with that of the original conditions at $z = 25$: they are almost identical.

The r.m.s wavenumber of the HI structures also remains approximately constant at $\langle k^2 \rangle^{1/2} \approx 0.7 \text{ Mpc}^{-1} h$ (corresponding to a characteristic scale $\langle \lambda^2 \rangle^{1/2} \approx 9 \text{ Mpc } h^{-1}$) during this epoch as can be seen in Figure 4. Again, this is characteristic of linear evolution, which does not change the topology in any way.

At the end of this phase, we begin to see a rise in the amplitude of the genus (see plot for $z = 15.7$ in Figure 2). This is an indication that the reionization is becoming more significant as HII bubbles begin to grow, leading to the next phase.

4.2. Pre-overlap; $10 \lesssim z \lesssim 16$; $0.63 \lesssim \bar{f}_{\text{HI}} \lesssim 0.96$

Starting at a redshift of $z \sim 15$, the topology starts to change appreciably as reionization begins in earnest.

The genus curves (e.g. the plot for $z = 15.7$ and $z = 12.1$ in Figure 2) start to display an asymmetry between low- and high- ν portions: while the absolute value of the genus for intermediate and high density regions ($\nu > 0$) increase along with the overall amplitude, the curve flattens out at low ν , and the absolute genus values at these densities decrease.

A genus curve with this shape is not new: when Gott (11) studied the topologies of non-random phase distributions for the universe, one possibility they considered was one in which galaxies are distributed at surfaces surrounding large voids. This has striking similarities with the pre-overlap genus curves in the present case, indicating clearly that large ionized HII bubbles are being created during this epoch. However, in the present work, the bubbles have continuously varying HI densities in

contrast to the uniform voids studied in Gott (11). Indeed, the increase of the absolute value of the genus towards the median ($\nu = 0$) in the $\nu < 0$ regime is indicative of the intuitive fact that the most highly ionized bubbles are rarer than less ionized ones, thus less bubbles are detected at the lowest threshold densities. Also, the topology at high densities is different in both cases. In Gott (11), the galaxies were distributed randomly on the bubble walls (and hence approximately uniformly), while in the present case of pre-overlap reionization the high density regions outside of the ionized bubbles still have an approximately Gaussian distribution of neutral hydrogen.

From Figure 3a, we see that the curves relating threshold density $\rho_{\text{thres, HI}}/\langle\rho_{\text{H}}\rangle$ to a given volume fraction f or ν have a different shape during this epoch, with a straight line at $\nu \gtrsim 0$, but with a tail dropping off steeply towards low HI densities at low ν , a characteristic which becomes increasingly marked with decreasing redshift. This can also be seen in Figure 3b, in which the threshold density for low volume fractions begin decreasing rapidly at around $z \sim 14$, while the threshold densities at median and high volume fractions decrease more gently. This is indicative of the drastic reduction in neutral density within the interiors of HII bubbles.

In Figure 5, a comparison between the contours at $z = 24.9$ and $z = 9.6$ reveals that regions initially occupied by high density contours have now become low density voids. For example, it is clear that the large high-density pocket near the middle front of the box in the initial conditions has become a low-density void. This is a strong indication of ‘inside-out’ reionization. In this picture, the highest density regions are the first in which halos can accrete sufficient mass (and hence virial temperatures of $T \gtrsim 10^4$) for atomic cooling to occur and cause the halos to collapse and commence star formation. These star-forming regions in turn becomes sources of ionizing flux, which ionize the surrounding neutral gas.

This effect means that the HII bubbles detected in the $\nu < 0$ part of the genus curve are in high-density regions which have been strongly ionized, and not regions with intrinsically low density.

During this stage, the ionizing fluxes are shielded from the IGM by virtue of being within dense regions with high recombination rates, hence the universe outside of the HII regions is little affected by reionization. Outside of the increasingly low HI densities in the HII bubbles, the relative densities are still the same. For example, a $\nu = -1.5$ void in the $z = 24.9$ distribution is by definition less dense than a $\nu = 0$ median density region during the same era, but they still have approximately the same relative densities with respect to each other during the pre-overlap stage of reionization as they experience little ionizing flux. The main difference is that the original dense pockets have become HII regions and are now voids with respect to the rest of the universe, so the volume fractions covered by the un-ionized regions have been reduced (i.e. ν increased). This can be seen by looking at the positions of the intermediate (green, $\nu = 0$) and dense (red, $\nu = 1.5$) density contours for $z = 9.6$ in Figure 5: the former are in regions formerly occupied by the voids while the latter are in regions once part of the sponge-like median density contour. The correspondence

between the contours in is not exact because the actual threshold density values for e.g. the $\nu = 1.5$ contour at $z = 9.6$ and $\nu = 0$ at $z = 24.9$ are not exactly matched to each other, but is sufficient to demonstrate the broad trends at different densities.

This argument is supported by the evolution of the threshold densities with redshift in Figure 3a. We see, in this context, that the low-density tail signifying HII bubbles must be from regions that used to be in the high- ν part of the curve in earlier times. The straight portion at $\nu \gtrsim 0$ is from regions that once occupied the low density $\nu \lesssim 0$ portion of the straight line representing the Gaussian distribution before reionization began. These have now been translated to occupy higher volume fractions relative to the overall distribution. However, even in these regions, some small amount of ionization is taking place at scales below the smoothing length, which slowly decrease the local HI densities.

As HII regions begin forming in the regions of highest baryon density, recombination initially mitigates the effects of the ionizing flux. Thus, these partially ionized regions initially appear as bubbles of intermediate neutral density growing within highly dense regions. This has the effect of creating holes and isolating individual dense clumps within the dense regions as the HII regions appear, breaking up the topology and increasing the amplitude of the genus.

As reionization progresses, the absolute genus value of the low-density regions decreases due to the merger of small HII bubbles into a smaller number of large bubbles (compare $\nu < -1$ tails of $z = 12.10$ and $z = 9.6$ in Figure 2). This is in agreement with Shin (21), which found that the majority of bubble mergers occur during this epoch.

4.3. *Overlap*; $8 \lesssim z \lesssim 10$; $0.26 \lesssim \bar{f}_{\text{HI}} \lesssim 0.63$

At $z \sim 9$, volume-weighted mean HI fraction of the universe drops to $\bar{f}_{\text{HI}} \lesssim 0.5$ (Figure 1), in contrast with the leisurely decrease in previous phases, even though there is merely a modest increase in the amount of ionizing flux emitted by the star-forming regions (now dominated by Pop II stars; see (author?)) (Trac & Cen 2006)). This sudden decrease occurs as the ionized bubbles overlap with each other, so that ionizing photons can now stream between previously isolated bubbles and increase the ionizing flux experienced by points within the overlapping ionized regions. This increased flux overcomes the effects of recombination and increases the ionization rate. At regions occupying the lowest volume fractions, the gas is essentially completely ionized, with $\rho_{\text{thres, HI}}/\langle\rho_{\text{H}}\rangle \lesssim 0.01$ at $\nu = -1.5$ (Figure 3b).

As the regions occupying the median volume fractions ($f = 0.5$ or $\nu \sim 0$) are now also part of significantly ionized regions, the genus of what were previously multiply-connected regions is now strongly suppressed due to the overlapping of HII regions, which closes gaps in the sponge-like contours (and hence reduces the positive genus). By $z = 9.6$, the overall amplitude of the genus curve is considerably lower than that at $z = 12.1$ (Figure 2). This reflects an increase in the characteristic scale of the neutral distribution, driving down the r.m.s. wavenumber and hence the genus amplitude (Figure 4). Immediately after $z \sim 9$, the topology of the distribution across all densities becomes strongly non-Gaussian

as can be seen from a comparison of the genus curves for $z = 9.6$ and $z = 8.2$ in Figure 2. After this point, there no longer exists large neutral structures with approximately Gaussian distributions within them. This means we can no longer estimate a characteristic scale using Equation 5 and so we truncate Figure 4 at $z \sim 9$.

The overlap of ionized regions means that the topology at low-densities is dominated by a small number of large interconnected regions, which is detected as $G_s \gtrsim 0$ in the $\nu < 0$ portion of the genus curve for $z = 8.2$ (Figure 2), and is seen in the corresponding contours in Figure 5.

With the percolation of HII bubbles through the IGM, the remaining regions with a relatively high HI density ($\rho_{\text{thres, HI}}/\langle\rho_{\text{H}}\rangle \gtrsim 0.5$ at $\nu > 0$) are now isolated into individual pockets (see the corresponding contours in Figure 5). This is also seen in the high-density $\nu \gtrsim 1.5$ portion in the genus curve for $z = 8.2$ in Figure 2, which retains vestiges of its curved Gaussian shape. This is because these high density regions are still shielded from the ionizing flux flooding the rest of the universe, thus within them the *relative* density distributions still reflect those of the initial conditions. But even within these pockets, small amounts of star formation are going on at scales below the smoothing length, which continue pushing down slowly on the densities. The stage is now set for the reionization of the remaining large-scale HI structures in the universe.

4.4. Post-overlap; $6 \lesssim z \lesssim 8$; $\bar{f}_{\text{HI}} \lesssim 0.26$

By redshifts of $z \sim 8$, the median HI density of universe is $\rho_{\text{thres, HI}}/\langle\rho_{\text{H}}\rangle \sim 0.1$ and dropping (Figure 3). The contours with threshold densities below the median, $\nu < 0$, are now almost thoroughly ionized, as characterised by the flat tails in the corresponding $\rho_{\text{thres, HI}}/\langle\rho_{\text{H}}\rangle$ v.s. ν plots in Figure 3a.

In the genus curve for $z = 7.3$ (Figure 2), the genus at $\nu < 0$ has now assumed a shape that appears similar to that of a Gaussian distribution, but truncated where it crosses the median volume fraction at $\nu \approx 0$. This indicates that regions below these threshold densities are totally ionized, with the unresolved neutral regions (i.e. galaxies) within them acting as tracers of the baryon's Gaussian random phase density distribution. A comparison with the curve in Figure 3 at this redshift concurs with the notion that a straight line in the $\rho_{\text{thres, HI}}/\langle\rho_{\text{H}}\rangle$ v.s. ν curve is indicative of a random phase distribution. At $0 \lesssim \nu \lesssim 1.5$, ionized regions have yet to be completely ionized, and have the topology of a unified region punctuated by small numbers of holes.

These holes are caused by the remaining resolved pockets of high-density HI in the universe, which by this epoch has a density about 2 orders of magnitude greater than fully ionized regions occupying most of the IGM (Figure 3b). These pockets can also be seen in the genus curve at $\nu \gtrsim 1.5$. However, the small negative amplitude of the genus indicates that only a small number of neutral pockets remain, and corresponding volume fraction they occupy is small ($f = 0.02$ at $\nu = 2$).

With the universe now largely ionized, most of the IGM has a low optical depth to ionizing photons. The remaining HI regions are isolated pockets occupying small volumes, which implies that they have relatively large surface areas exposed to large amounts of ionizing flux.

Under these circumstances, the final reionization of these pockets happen within a relatively short period of time as illustrated in Figure 3a, where $\rho_{\text{thres, HI}}/\langle\rho_{\text{H}}\rangle$ at $\nu \sim 1.5$ decreases by about 2 orders of magnitude during the interval $5.6 \lesssim z \lesssim 7$.

The genus curve at $z = 6.4$ (Figure 2) offers an interesting snapshot of the topology during this time. The curve at $\nu < 1$ is distinctively that of the Gaussian random-phase distribution, corresponding to the baryonic distribution traced by the unresolved neutral HI. At $\nu > 1$, we see that the densest $\sim 10\%$ ($f \sim 0.1$) of the volume are in a very tiny number of dense neutral pockets, but they no longer exist by $z = 5.6$.

At the end of post-overlap reionization at $z = 5.6$, the HI threshold density is a straight line with respect to ν (Figure 3a), with $\rho_{\text{thres, HI}}/\langle\rho_{\text{H}}\rangle \lesssim 0.01$. This indicates that the reionization of the universe is complete by this redshift, and the tiny amounts of neutral HI remaining in the universe now traces the overall baryon distribution in the universe, which is still Gaussian random phase to a good approximation. This is supported by the corresponding genus curves (Figure 2) and contours (Figure 5)).

We note that a post-reionization Gaussian random-phase distribution is directly supported by observational evidence: Weinberg (27) had studied the 1-dimensional topology of neutral hydrogen using Ly- α absorption lines in quasars with $z \lesssim 2.5$, and it was found that the distribution of threshold crossings as a function of ν (i.e. number of threshold crossings $\propto \exp(-\nu^2/2)$) smoothed on scales of $1 \text{ Mpc } h^{-1}$ is consistent with a Gaussian random-phase distribution .

In the contours plots, the distribution of the high- and low-density regions at $z = 5.6$ bear a resemblance to the initial conditions at $z = 24.9$. For example, the anvil-shaped void at the top vertex facing the reader can clearly be matched with an similarly-shaped object in the initial conditions, as is the small void at the lower vertex. In general, the contour distributions in the initial and post-reionization volume can be approximately matched to each other, but there are small differences.

The post-reionization universe is in general choppier than the initial conditions, most noticeably in the dense regions. This is supported by a comparison between the two corresponding genus curves (Figure 2). The amplitude of the genus curve at $z = 5.6$ is about twice that at $z = 24.9$, giving a corresponding decrease in the characteristic wavelength according to Equation 5. This difference is most likely due to non-linear effects which occurred in the baryon distribution whilst reionization was taking place, but is beyond the scope of this paper.

5. CONCLUSION

We use a state-of-the-art cosmological reionization simulation to quantify the topology of cosmological reionization, using genus curve measurements of the neutral hydrogen density distribution on $\geq 1 \text{ Mpc } h^{-1}$ scales. Overall, the reionization process begins in an inside-out fashion on scales, where higher density regions become ionized earlier than lower density regions. Reionization finally completes when the isolated neutral structures which remain are reionized in from outside-in.

The sequence of topological transitions can be mapped to four phases:

(1) pre-reionization: $z \gtrsim 15$, (2) pre-overlap: $10 \lesssim z \lesssim 15$, (3) overlap: $8 \lesssim z \lesssim 10$, (4) post-overlap: $6 \lesssim z \lesssim 8$.

In Phase (1) the genus curve is consistent with a Gaussian density distribution and topology remains unchanged as the universe evolves via linear evolution. In Phase (2) the number of HII bubbles increases gradually with time, coincident with the increase in the amplitude of the genus curve. Most of this occurs in the highest density regions which begin star-formation earlier. At the later stages of this phase, HII bubbles start to merge/percolate, resulting in a turn-over and subsequent decrease in the amplitude of the genus curve. An isolated HII-bubble dominated topology is evident in the genus curve during this phase. In Phase (3) the HII bubbles rapidly merge, manifested by the precipitous drop in the amplitude of the genus curve. The reionization of the IGM occurs rapidly as the ionizing photons are now free to stream freely between connected HII re-

gions, increasing local ionizing fluxes. In Phase (4) the IGM is thoroughly ionized and the genus curve is consistent with an increasingly diminishing number of isolated neutral islands, with the reionization of the universe at $\sim 1 \text{ Mpc } h^{-1}$ complete by a redshift of $z \approx 6$.

These results represent a concrete identification of the redshifts at which the different epochs of reionization occur, and elucidates the evolution of the neutral topology.

This work is supported in part by grants AST-0407176 and NNG06GI09G. HT is supported in part by NASA grant LTSA-03-000-0090. JRG is supported by grant AST-04-06713. We thank Min-Su Shin for useful discussions and advice. We are grateful to the referee, Nick Gnedin, for his constructive criticisms and suggestions which have improved the paper.

REFERENCES

- Adler, R. J. 1981, *The Geometry of Random Fields* (The Geometry of Random Fields, Chichester: Wiley, 1981)
- Bardeen, J. M., Bond, J. R., Kaiser, N., & Szalay, A. S. 1986, *ApJ*, 304, 15
- Bardeen, J. M., Steinhardt, P. J., & Turner, M. S. 1983, *Phys. Rev. D*, 28, 679
- Barkana, R. 2002, *New Astronomy*, 7, 85
- Barkana, R. & Loeb, A. 2001, *Phys. Rep.*, 349, 125
- Becker, R. H., Fan, X., White, R. L., Strauss, M. A., Narayanan, V. K., Lupton, R. H., Gunn, J. E., Annis, J., et al. 2001, *AJ*, 122, 2850
- Canavezes, A., Springel, V., Oliver, S. J., Rowan-Robinson, M., Keeble, O., White, S. D. M., Saunders, W., Efstathiou, G., et al. 1998, *MNRAS*, 297, 777
- Cen, R. 2003, *ApJ*, 591, 12
- Cen, R. & McDonald, P. 2002, *ApJ*, 570, 457
- Chiu, W. A., Fan, X., & Ostriker, J. P. 2003, *ApJ*, 599, 759
- Doroshkevich, A. G. 1970, *Astrophysics*, 6, 320
- Fan, X., Narayanan, V. K., Strauss, M. A., White, R. L., Becker, R. H., Pentericci, L., & Rix, H.-W. 2002, *AJ*, 123, 1247
- Furlanetto, S. R., Zaldarriaga, M., & Hernquist, L. 2004, *ApJ*, 613, 1
- Gnedin, N. Y. 2000a, *ApJ*, 535, 530
- . 2000b, *ApJ*, 542, 535
- Gott, III, J. R., Dickinson, M., & Melott, A. L. 1986, *ApJ*, 306, 341
- Gott, J. R. I., Hambrick, D. C., Vogeley, M. S., Kim, J., Park, C., Choi, Y.-Y., Cen, R., Ostriker, J. P., et al. 2006, *ArXiv Astrophysics e-prints*
- Gott, J. R. I., Miller, J., Thuan, T. X., Schneider, S. E., Weinberg, D. H., Gammie, C., Polk, K., Vogeley, M., et al. 1989, *ApJ*, 340, 625
- Gott, J. R. I., Weinberg, D. H., & Melott, A. L. 1987, *ApJ*, 319, 1
- Haiman, Z., Abel, T., & Madau, P. 2001, *ApJ*, 551, 599
- Hamilton, A. J. S., Gott, J. R. I., & Weinberg, D. 1986, *ApJ*, 309, 1
- Holder, G. P., Haiman, Z., Kaplinghat, M., & Knox, L. 2003, *ApJ*, 595, 13
- Lidz, A., Hui, L., Zaldarriaga, M., & Scoccimarro, R. 2002, *ApJ*, 579, 491
- Mackey, J., Bromm, V., & Hernquist, L. 2003, *ApJ*, 586, 1
- Madau, P. 2002, in *Astronomical Society of the Pacific Conference Series*, Vol. 283, *A New Era in Cosmology*, ed. N. Metcalfe & T. Shanks, 318–+
- McQuinn, M. & Lidz, A. & Zahn, O. & Dutta, S. & Hernquist, L. & Zaldarriaga, M. 2007, *MNRAS*, 377, 1043
- Miralda-Escudé, J., Haehnelt, M., & Rees, M. J. 2000, *ApJ*, 530, 1
- Moore, B., Frenk, C. S., Weinberg, D. H., Saunders, W., Lawrence, A., Ellis, R. S., Kaiser, N., Efstathiou, G., et al. 1992, *MNRAS*, 256, 477
- Peacock, J. 1992, *Nature*, 355, 203
- Rees, M. J. 1998, *Proceedings of the National Academy of Science*, 95, 47
- Ricotti, M. & Ostriker, J. P. 2004, *MNRAS*, 350, 539
- Ryden, B. S., Melott, A. L., Craig, D. A., Gott, J. R. I., Weinberg, D. H., Scherrer, R. J., Bhavsar, S. P., & Miller, J. M. 1989, *ApJ*, 340, 647
- Seifert, H. & Threlfall, W. ; translated by Goldman, W. A. 1980, *A textbook of topology, Pure and applied mathematics, a series of monographs and textbooks* (New York : Academic Press)
- Shin, M. S., Trac, H., & Cen, R. 2007, *ApJ*, submitted
- Somerville, R. S., Bullock, J. S., & Livio, M. 2003, *ApJ*, 593, 616
- Spiegel, D. N., Bean, R., Dore, O., Nolta, M. R., Bennett, C. L., Hinshaw, G., Jarosik, N., Komatsu, E., et al. 2006, *ArXiv Astrophysics e-prints*
- Spiegel, D. N., Verde, L., Peiris, H. V., Komatsu, E., Nolta, M. R., Bennett, C. L., Halpern, M., Hinshaw, G., et al. 2003, *ApJS*, 148, 175
- Trac, H. & Cen, R. 2006, *ArXiv Astrophysics e-prints*
- Trac, H. & Pen, U.-L. 2006, *New Astronomy*, 11, 273
- Venkatesan, A. & Truran, J. W. 2003, *ApJ*, 594, L1
- Venkatesan, A., Tumlinson, J., & Shull, J. M. 2003, *ApJ*, 584, 621
- Vogeley, M. S., Park, C., Geller, M. J., Huchra, J. P., & Gott, J. R. I. 1994, *ApJ*, 420, 525
- Weinberg, D. H. 1988, *PASP*, 100, 1373
- Weinberg, D. H., Burles, S., Croft, R. A. C., Dave, R., Gomez, G., Hernquist, L., Katz, N., Kirkman, D., et al. 1998, *ArXiv Astrophysics e-prints*
- Wyithe, J. S. B. & Loeb, A. 2003, *ApJ*, 586, 693
- Zahn, O. & Lidz, A. & McQuinn, M. & Dutta, S. & Hernquist, L. & Zaldarriaga, M. & Furlanetto, S. R. 2007, *ApJ*, 654, 12